Structural Mechanism of Enoyl-CoA Hydratase: Three Atoms from a Single Water Are Added in either an E1cb Stepwise or Concerted Fashion[†,‡]

Brian J. Bahnson,*[,§] Vernon E. Anderson,[||] and Gregory A. Petsko[⊥]

Department of Chemistry and Biochemistry, University of Delaware, Newark, Delaware 19716, Department of Biochemistry, Case Western Reserve University, Cleveland, Ohio 44106, and Rosenstiel Center, Brandeis University, Waltham, Massachusetts 02254

Received October 9, 2001; Revised Manuscript Received December 7, 2001

ABSTRACT: We have determined the crystal structure of the enzyme enoyl-CoA hydratase (ECH) from rat liver with the bound substrate 4-(*N*,*N*-dimethylamino)cinnamoyl-CoA using X-ray diffraction data to a resolution of 2.3 Å. In addition to the thiolester substrate, the catalytic water, which is added in the hydration reaction, has been modeled into well-defined electron density in each of the six active sites of the physiological hexamer within the crystallographic asymmetric unit. The catalytic water bridges Glu^{144} and Glu^{164} of the enzyme and has a lone pair of electrons poised to react with C_3 of the enzyme-bound α,β-unsaturated thiolester. The water molecule, which bridges two glutamate residues, is reminiscent of the enolase active site. However, unlike enolase, which has a lysine available to donate a proton, there are no other sources of protons available from other active site residues in ECH. Furthermore, an analysis of the hydrogen-bonding network of the active site suggests that both Glu^{144} and Glu^{164} are ionized and carry a negative charge with no reasonable place to have a protonated carboxylate. This lack of hydrogen-bonding acceptors that could accommodate a source of a proton, other than from the water molecule, leads to a hypothesis that the three atoms from a single water molecule are added across the double bond to form the hydrated product. The structural results are discussed in connection with details of the mechanism, which have been elucidated from kinetics, site-directed mutagenesis, and spectroscopy of enzyme−substrate species, in presenting an atomic-resolution mechanism of the reaction. Contrary to the previous interpretation, the structure of the E−S complex together with previously determined kinetic isotope effects is consistent with either a concerted mechanism or an E1cb stepwise mechanism.

Enoyl-CoA hydratase (ECH,[1] EC 4.2.1.17), also known as crotonase, catalyzes the *syn* addition (*1*) of water across the double bond of α,β-unsaturated thiolesters, which is the second step of the β-oxidation of fatty acids. Many details of the catalytic power of this enzyme have been elucidated by kinetics and spectroscopy. After thorough investigations utilizing kinetic isotope effects (*2*, *3*), the mechanism of the addition reaction has been proposed to involve a concerted reaction where both the C−H and C−O bonds are formed in a single chemical step as shown in Scheme 1. We sought to obtain a structure of a productive enzyme−substrate (E−S) complex to gain a structural perspective to combine with solution information obtained from kinetics, mutagenesis, and spectroscopy of E−S complexes.

Scheme 1: Reaction Catalyzed by ECH

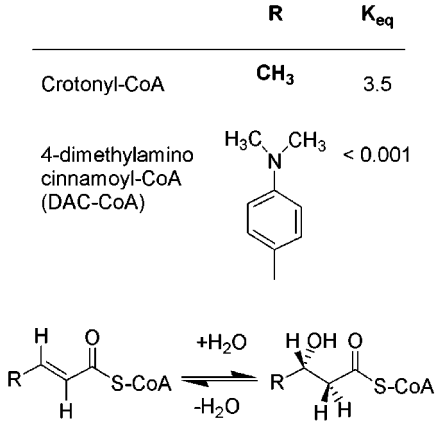

The crystal structure of ECH was initially determined with the competitive inhibitor acetoacetyl-CoA bound (*4*). This structure confirms predictions about which residues are involved in acid−base catalysis and polarization of the thiolester carbonyl (*5*−*7*). However, the complex with this inhibitor does not provide a precise picture of how each residue in the enzyme's active site sets up the addition reaction. This could only be shown with a true E−S complex.

We have determined the crystal structure of ECH complexed with the substrate 4-(*N*,*N*-dimethylamino)cinnamoyl-

[†] The research was partially supported by a grant from the NIH (GM 36562) to V.E.A.

[‡] Coordinates for the structure of enoyl-CoA hydratase complexed with the substrate 4-(*N*,*N*-dimethylamino)cinnamoyl-CoA have been deposited in the Protein Data Bank as entry 1EY3.

* To whom correspondence should be addressed. E-mail: bahnson@udel.edu. Telephone: (302) 831-0786. Fax: (302) 831-6335.

[§] University of Delaware.

[||] Case Western Reserve University.

[⊥] Brandeis University.

[1] Abbreviations: *B*-factor, temperature factor; DAC-CoA, 4-(*N*,*N*-dimethylamino)cinnamoyl-CoA; ECH, enoyl-CoA hydratase; E−P, enzyme−product; E−S, enzyme−substrate; R_{free}, free *R*-factor; $R_{working}$, working *R*-factor; QM/MM, quantum-mechanics/molecular-mechanics.

10.1021/bi015844p CCC: $22.00
Published on Web 01/29/2002

CoA (DAC-CoA). The determination of this structure by X-ray crystallography was possible because the conjugation of the aromatic group to the α,β-unsaturated enoyl group in the DAC-CoA molecule shifts the equilibrium toward the E−S complex (Scheme 1). Despite the >1000-fold thermodynamic preference for the unsaturated substrate, the enzyme has been shown to catalyze the dehydration of 3-hydroxy-3-phenylpropanoyl-CoA to cinnamoyl-CoA, with a rate comparable to that of the physiological substrates (*8*), thereby indicating the physiological relevance of this E−S structure.

Cinnamoyl-CoA substrates are particularly attractive targets for structural and spectroscopic studies due to the π-conjugation of the α,β-unsaturated thiol ester. The aromatic conjugation limits the potential conformers, both in solution and bound at the active site. Previously, the ^{13}C NMR spectroscopy of cinnamoyl-CoA bound to ECH showed that C_1 and C_3 had decreased shielding and C_2 had increased shielding (*9*). Spectroscopic information such as the ^{13}C NMR shifts of E−S complexes can be further analyzed with structural information, thereby allowing a complete description of electrostatic interactions that are responsible for substrate polarization and, ultimately, catalysis. The structure reported in this paper of a single E−S conformer was a critical component of interpreting the ^{13}C NMR spectra of a true E−S complex, as was done by D'Ordine et al., in the following paper (*10*).

The structure of the enzyme with the substrate bound shows a simple approach that has evolved for achievement of catalysis of its reaction near the diffusion limit (*11*). There has been considerable interest in understanding the chemistry that differs between the *anti* and a *syn* addition−elimination reactions (*12*, *13*). The observation of an E−S complex provides a detailed description of the residues that interact with the substrate thiolester and water. Furthermore, the H-bonding environment uniquely suggests a mechanism that is consistent with all previously measured kinetic and spectroscopic data. Together, the ECH·DAC-CoA structure suggests a rationale for why this enzyme's reaction is a *syn* addition by the nature of how the three atoms of a single water molecule are set up to add to the double bond of the substrate. To our surprise, this unique approach of catalysis opens up the possibility that the reaction proceeds with a stepwise mechanism, and yet is consistent with all previously measured kinetic isotope effects (*2*, *3*).

EXPERIMENTAL PROCEDURES

Preparation of ECH. Recombinant rat liver ECH was expressed from a pET expression plasmid in *Escherichia coli* as described previously (*5*). The protein was purified from the resulting supernatant by crystallization upon addition of ethanol, while cooling in a dry ice/ethanol bath, followed by incubation at 4 °C for 48 h. The resulting white precipitate was centrifuged and dialyzed before loading onto a CoA-Sepharose affinity column. Fractions containing ECH were combined, and ECH was concentrated and further purified by a recrystallization step using 10% ethanol and stored at −20 °C. The concentration of ECH was estimated using UV spectroscopy and a molar extinction coefficient of 16 000 M^{-1} cm^{-1} at 280 nm (*14*).

Crystal Growth and Data Collection for ECH·DAC-CoA. A solution of ECH was prepared at a concentration of 0.5 mM active sites (14 mg/mL) in 75 mM sodium phosphate, 100 mM NaCl, and 3 mM sodium azide, at a final pH of 7.3. DAC-CoA was added to the protein solution to a final concentration of 3.5 mM. This solution was filtered through a 0.2 μm cellulose acetate filter. Initial crystallization conditions were obtained using the incomplete factorial analysis technique (*15*). Diffraction quality crystals of the DAC-CoA complex were grown at 25 °C via vapor diffusion using the hanging drop method. Individual drops were prepared by microseeding 10 μL hanging drops (5 μL of a protein stock and 5 μL of the reservoir solution) that were equilibrated against a reservoir solution of 8% PEG 4000, 0.1 M NaOAc, and 75 mM sodium phosphate (pH 7.3). Diffraction data were collected at 2 °C from one crystal on an R-AXIS II detector with a Cu rotating anode source running at 50 kV and 145 mA, and were processed with DENZO and SCALEPACK software (*16*).

Crystal Structure Solution and Refinement. The structure was initially phased following molecular replacement using the CCP4 program AMORE (*17*), starting with a model from the 2.5 Å resolution structure of ECH (PDB entry 1DUB) with the competitive inhibitor acetoacetyl-CoA bound (*4*). The model used for the molecular replacement search was the hexamer without the bound inhibitor. Following molecular replacement, the model was subjected to refinement using the program XPLOR (*18*). Rigid body refinement was performed for 50 cycles. Initially, noncrystallographic constraints were enforced in the model, where each of the six monomers in the asymmetric unit was forced to be identical. Simulated annealing from a starting temperature of 3000 °C improved the model, as shown by a lower free *R*-factor (R_{free}) (*19*). The model was then subjected to 25 rounds of positional refinement and was adjusted using the graphics program O (*20*) to fit into the initial electron density maps ($3F_o - 2F_c$ coefficients). Further positional refinement was performed with noncrystallographic restraints applied between the six similar monomers in the asymmetric unit. The substrate DAC-CoA was built into each of the six active sites within the hexamer of the enzyme using electron density maps with the $2F_o - F_c$ coefficients. Refinement was performed using diffraction data from 8 to 2.3 Å, with alternate rounds of positional refinement, individual temperature factor (*B*-factor) refinement, water building, and model adjustment until the refinement converged as judged by the R_{free} value. Geometry was assessed and corrected using the CCP4 program PROCHECK (*17*). Unfavorable regions of the model were corrected manually, the result being that the six monomers in the asymmetric unit had similar backbone geometry.

The E−S model was then refined using the CNS program (*21*). All the data between a resolution of 30 and 2.3 Å were used in the subsequent refinement with a bulk solvent correction applied. The wat_pick feature of CNS was used to select water molecules on the basis of omit maps with the $F_o - F_c$ coefficients, hydrogen-bonding geometry, and refined *B*-factors. Waters without a reasonable hydrogen-bonding environment or with a *B*-factor of >60 $Å^2$ were removed. Several rounds of water generation and removal were repeated with intermittent rounds of positional and individual *B*-factor refinement. The final round of refinement was performed with noncrystallographic restraints set at a low force constant. The model was determined to be

Table 1: Crystal Structure Determination of the ECH·DAC-CoA Complex

data collection	
space group	$P2_12_12_1$
cell parameters	
a (Å)	141.6
b (Å)	145.4
c (Å)	78.6
no. of monomers/asymmetric unit	6
resolution (Å)	30.0−2.3
completeness (%)	95
R_{merge}[a]	0.062
refinement	
resolution range (Å)	30.0−2.3
$R_{working}$[b]	0.18
R_{free}[b]	0.22
observed rms deviations	
bond lengths (Å)	0.007
bond angles (deg)	1.2
total no. of non-hydrogen atoms	12642
total no. of water molecules	486

[a] $R_{merge} = \sum|I_o - I_a|/\sum(I_a)$, where I_o is the observed intensity and I_a is the average intensity, the sums being taken over all symmetry-related reflections. [b] *R*-factor $= \sum|F_o - F_c|/\sum(F_o)$, where F_o is the observed amplitude and F_c is the calculated amplitude. R_{free} is the equivalent of $R_{working}$, except it is calculated for a randomly chosen set of reflections that were omitted (10%) from the refinement process (*19*).

complete when all further attempts at model adjustment and refinement failed to reduce the R_{free} (*19*).

RESULTS

The crystal structure of ECH with DAC-CoA bound represents a true E−S complex, thus adding a structural perspective to addressing unresolved details of the enzyme's mechanism. The crystals of ECH with the substrate DAC-CoA bound grew with the symmetry of the orthorhombic space group $P2_12_12_1$ with the following unit cell dimensions: $a = 141.6$ Å, $b = 145.4$ Å, and $c = 78.6$ Å. Statistics of the crystal structure solution and refinement are summarized in Table 1. This crystal form has one physiological hexamer of 168 kDa in the asymmetric unit. Therefore, the model presented here includes six independent views of the ECH active site with the bound substrate DAC-CoA, the catalytic water molecule, and each of the enzyme's active site residues that are critical for catalysis. The final model of ECH complexed with DAC-CoA has a working *R*-factor of 18% and an R_{free} of 22%. The Ramachandran plot of the ECH·DAC-CoA complex has 90% of the non-glycine and non-proline residues in the most favored regions and the remaining 10% in the additionally allowed regions, further indicating that this structure represents a good quality model. The overall structure of ECH with DAC-CoA bound is nearly identical to previously reported inhibitor-bound structures of ECH (*4*, *22*), with a few notable differences that will be highlighted below.

DAC-CoA Binding to ECH. The functional hexamer of ECH is made up of two stacked trimers. Each subunit contains an active site with minimal contacts[2] to bound CoA ligands from a neighboring subunit. The location of three bound DAC-CoA molecules can be seen in the trimer shown in Figure 1.

[2] The residues K260, F279, and K282 from a neighboring subunit have interactions with the adenosine portion of CoA thiolesters. F263 contacts the phenyl ring of the DAC-CoA substrate.

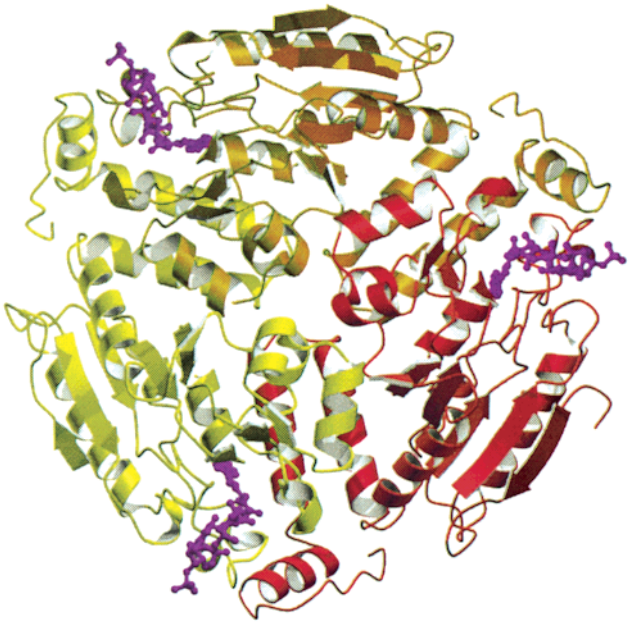

FIGURE 1: Trimer of ECH with one molecule of DAC-CoA bound per subunit shown in purple. Three identical monomers of 28 kDa (red, orange, and yellow) form one of the two trimers that are stacked to form the physiological hexamer (168 kDa). The resulting enzyme has six nearly identical active sites (three of these six are shown). This figure was created using the programs MOLSCRIPT (*23*), POVSCRIPT (E. Peisach and D. Peisach, unpublished program), and POVRAY (http://www.povray.org).

The diffraction data were phased by a molecular replacement solution starting from a model of ECH that had been determined with acetoacetyl-CoA bound (*4*). The model used in the molecular replacement lacked the bound inhibitor. Initial rounds of refinement were carried out in the absence of any bound ligands. Difference maps with $2F_o - F_c$ coefficients clearly showed strong electron density in each of the six active sites of the hexamer, allowing the DAC-CoA substrate to be built in unambiguously. The final structure shows well-defined electron density for all six bound molecules of DAC-CoA as shown in Figure 2 for subunit A. The substrate DAC-CoA is bound in the ECH active site in an *s-cis* conformation about the C_1-C_2 bond. The electron density is consistent with a single conformation of the DAC-CoA molecule for each of the six observed active sites. The average *B*-factor of 28 Å^2 for the (dimethylamino)-cinnamoyl portion of DAC-CoA is likewise consistent with a single well-ordered conformation of the substrate in the E−S structure. As expected, residues Glu^{144} and Glu^{164} are located in the proximity of the C_2-C_3 double bond of the DAC-CoA molecule. Also, residues Gly^{141} and Ala^{98} have hydrogen bond interactions with the carbonyl oxygen of the thiolester. With the exception of the residues noted above, there is a distinct lack of polar residues within 10 Å of the α,β-unsaturated thiolester moiety of the DAC-CoA substrate. Hydrophobic interactions with several residues make up the remainder of the ECH active site (M103, L117, W120, and F263 from a neighboring subunit).

Catalytic Water Poised for Reaction. Following the addition of DAC-CoA to the refined model, a clear electron density appeared in each of the six active sites of the hexamer among Glu^{144}, Glu^{164}, and C_3 of the substrate DAC-CoA as shown in Figure 2. This electron density was interpreted as

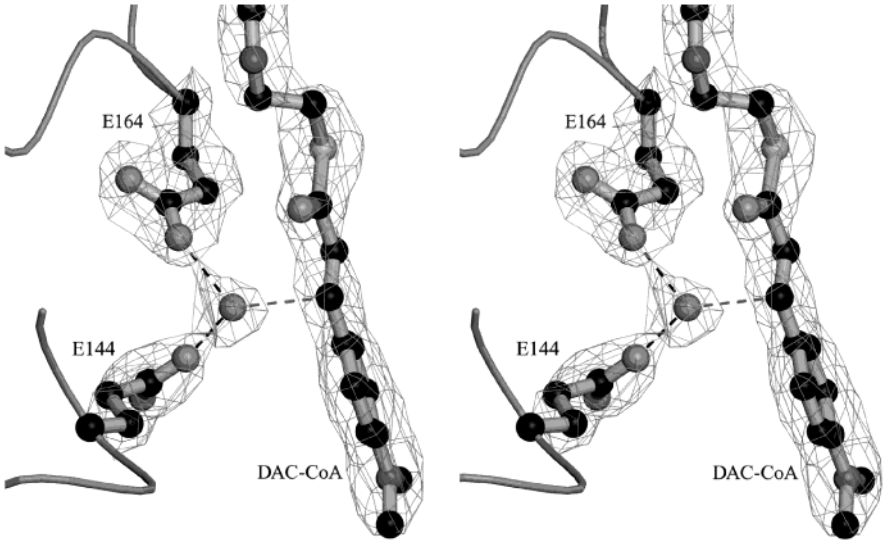

FIGURE 2: Stereoview of an annealed omit electron density map ($2F_o - F_c$) of the active site of ECH with DAC-CoA bound. The annealed omit map was generated following the omission of an 8 Å sphere from the catalytic water, followed by simulated annealing. The catalytic water that is added to the double bond of the DAC-CoA substrate is shown coordinated to Glu^{144} and Glu^{164}. The incipient C−O bond, which is formed in the addition reaction, is depicted by the gray dashed line between the catalytic water and C_3 of DAC-CoA. This figure was created using the programs MOLSCRIPT (*23*), POVSCRIPT (E. Peisach and D. Peisach, unpublished program), and POVRAY (http://www.povray.org).

the catalytic water and was built into this electron density in all six active sites with a final refined average *B*-factor of 26 $Å^2$. The simulated annealing omit electron density map shown in Figure 2 has been generated following the omission of a sphere of atoms 8 Å from the catalytic water and a round of simulated annealing. The active site electron density in the simulated annealing omit map is well-defined for all residues involved in catalysis and the bound substrate, thereby allowing a detailed analysis of interactions of this Michaelis complex.

The model of the two glutamates, the catalytic water, and the bound substrate is well-defined by the electron density (Figure 2), which is particularly critical to mechanistic interpretation. The hydrogen-bonding interactions of the catalytic water and of residues Glu^{144} and Glu^{164} are shown in Figure 3. The two hydrogen atoms of the catalytic water bridge the Glu^{144} and Glu^{164} carboxylate oxygens. The other two carboxylate oxygens of Glu^{144} and Glu^{164}, which are not interacting with the water, each accept two hydrogen bonds from amide nitrogens. For Glu^{144}, the hydrogen-bonding donors are the backbone NH group of Ala^{173} and Gly^{175}, while for Glu^{164}, the two amide donors are the backbone NH group of Glu^{164} (intraresidue) and the side chain amide of Gln^{162}. It was apparent that the carboxylate oxygen of Glu^{164} interacts with the ϵ-NH_2 group of Gln^{162}. The other heteroatom of the Gln^{162} side chain is H-bonded to the backbone NH group of Glu^{144}, requiring it to be the carbonyl oxygen of Gln^{162}. The side chain amide group of Gln^{162} also donates a hydrogen bond to the other carboxylate oxygen of Glu^{164} that is directly interacting with the catalytic water molecule. The catalytic water molecule has three H-bonding partners, the two glutamate carboxylates and the backbone NH group from Gly^{172}. The electron pair of the fourth tetrahedral position of the water molecule is directed toward C_3 of DAC-CoA, which is the position that forms the C−O bond in the reaction. A closer look at the interactions of the catalytic water reveals that the hydrogen bond that it donates to Glu^{164} is to the *anti* electron pair of the carboxylate oxygen versus the more basic *syn* electron pair of Glu^{144} (*24*, *25*). The closest carboxylate oxygen of Glu^{164} to the DAC-CoA substrate is 4.2 Å from C_2, which is the position of proton addition in the hydration reaction.

Polarization of the Substrate Carbonyl. The carbonyl of DAC-CoA accepts two hydrogen bonds from the backbone NH atoms of Gly^{141} and Ala^{98} each with a hydrogen bond distance of 2.9 Å as shown in Figure 4. The polarizing interaction with Gly^{141} is enhanced due to this residue's position at the N-terminus of an α-helix (*26*). Aside from the hydrogen bonding to the carbonyl, the acyl portion of the thiolester substrate is positioned within the ECH active site by hydrophobic interactions (M103 and I100).

The Mobile Loop Enables R Group Binding. The hydrophobic R group of the thiolester substrate has interactions with several hydrophobic residues as shown in Figure 5. The crystal structure of ECH with the competitive inhibitor acetoacetyl-CoA bound (*4*) is shown superimposed over the ECH·DAC-CoA structure. To bind the DAC-CoA substrate, the mobile loop, which includes residues 113−119 of each subunit, moves out of the way with a 3 Å displacement of Leu^{117}. A noteworthy observation of the R group binding of DAC-CoA is that the plane of the phenyl ring is not coplanar with the carbonyl and α,β-unsaturated moiety. The $C_2-C_3-C_4-C_5$ torsion angle varied from 12° to 29° among the six subunits observed in the E−S structure, compared to a gas phase calculation that shows a planar orientation about this bond for DAC-CoA (*10*).

DISCUSSION

The observations made from the ECH·DAC-CoA structure are applicable to a mechanistic understanding of reactions of the physiological saturated fatty acid thiolester substrates. It is generally more complicated to model the E−S complex for ECH using the physiological substrates that have an equilibrium constant near unity (*27*). Any crystal structures determined would be a mixture of an E−S and enzyme−

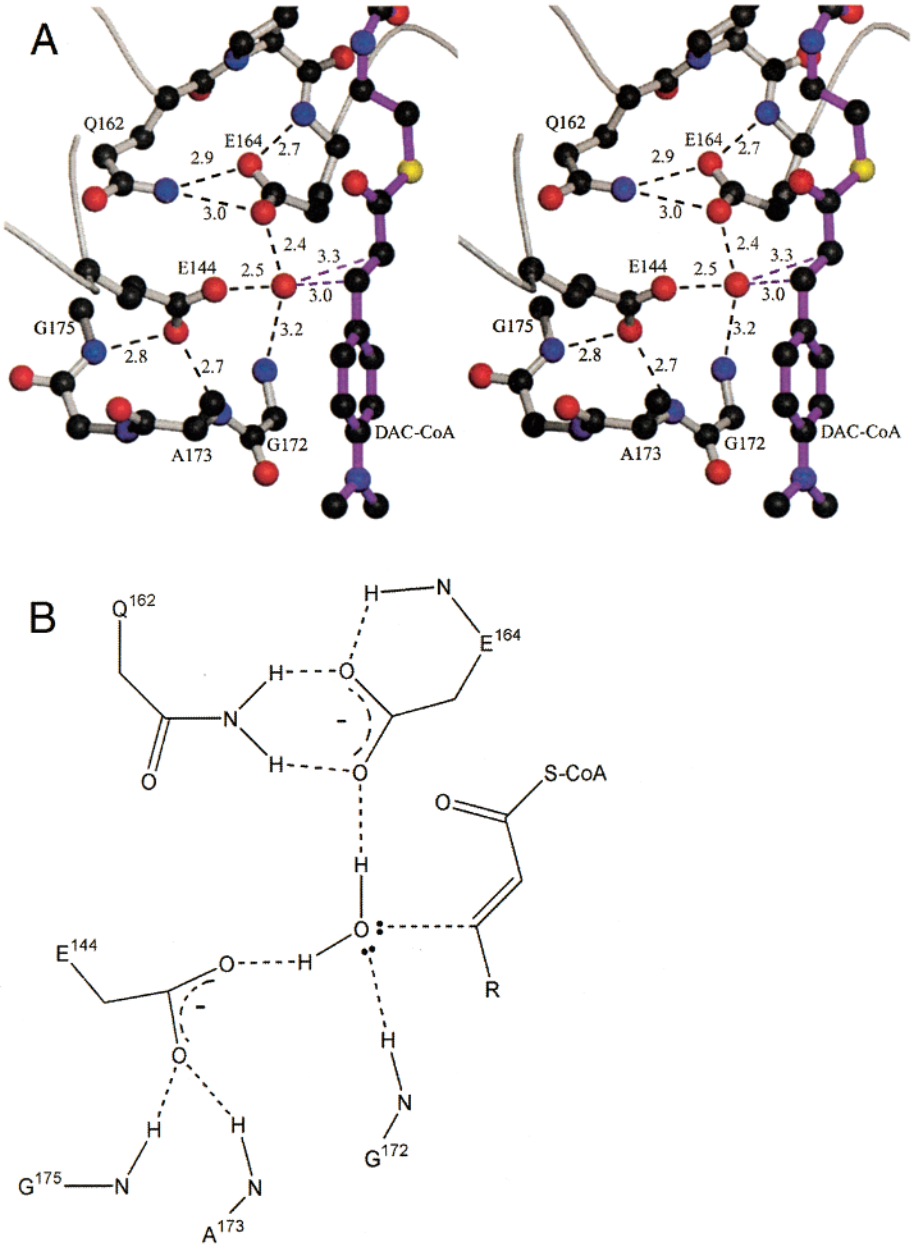

FIGURE 3: (A) Stereoview of the active site of ECH with DAC-CoA bound. The distances in units of angstroms are displayed for interactions near the catalytic water. Hydrogen bonds between the water and Glu[164], Glu[144], and Gly[172] (backbone NH group) are shown as black dashed lines. The distances between the catalytic water and either C_2 or C_3 of DAC-CoA are shown as purple dashed lines. The protein hydrogen-bonding partners of Glu[164] and Glu[144] are also displayed with black lines. This panel was created using the programs MOLSCRIPT (*23*), POVSCRIPT (E. Peisach and D. Peisach, unpublished program), and POVRAY (http://www.povray.org). (B) Schematic of hydrogen bonding which displays the placement of hydrogens and free lone pairs of the catalytic water.

product (E−P) complex. There have been several cases where alternate conformers of side chains or substrates and/or products have been modeled and refined (*28*−*31*). These can sometimes suffer from over-refinement and uncertainty of atomic details without adequate experimental data from crystals that diffract to a resolution limit of >1.8 Å. After all, in addition to alternate conformers for the substrate and product, the protein structure would likely vary between the E−S and E−P species. In light of the current limit of resolution of 2.3 Å for ECH crystal structures, a refinement that involves alternate conformers of a substrate and/or product would suffer from problems of over-refinement. In our current approach with ECH, we have determined the structure of a thermodynamically favored form that removes the uncertainty of multiple bound forms. In future work, we will attempt to collect data to sufficient resolution to enable a reliable refinement of a simultaneous E−S and E−P crystal structure with a substrate like crotonyl-CoA, which has an equilibrium constant closer to unity. Regardless, we feel the current model is representative of the true physiological E−S structure for the following reasons. Due to the thermodynamic preference, DAC-CoA is bound to the enzyme in high occupancy in the E−S form. The conjugation of an aromatic group in DAC-CoA stabilizes the α,β-unsaturated substrates to shift the equilibrium constant by >1000-fold (*32*). Despite the thermodynamic preference for the aromatic conjugated unsaturated substrate, the enzyme has been shown to catalyze the dehydration of 3-hydroxy-3-phenylpropanoyl-CoA to

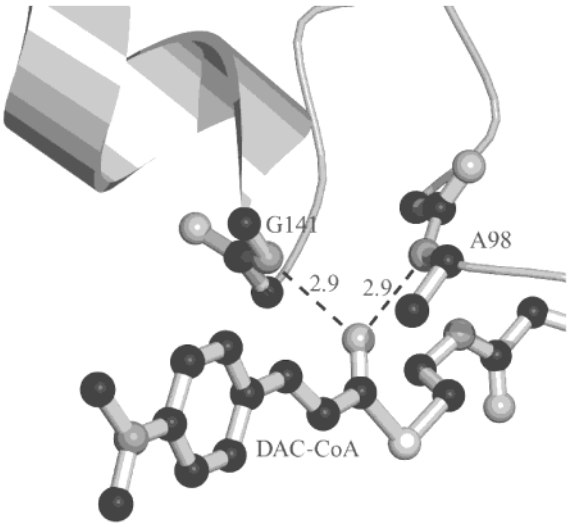

FIGURE 4: Carbonyl of the thiolester of DAC-CoA polarized by its coordination to the amide nitrogens of Ala^{98} and Gly^{141}. The N-terminus of the α-helix increases the partial positive charge for the NH group of Gly^{141}, thereby strengthening its polarizing interaction (*26*). This figure was created using the programs MOLSCRIPT (*23*), POVSCRIPT (E. Peisach and D. Peisach, unpublished program), and POVRAY (http://www.povray.org).

cinnamoyl-CoA, which is the reverse of the reaction depicted in Scheme 1. This reaction serves as a model of the hydrated form of the para-substituted DAC-CoA substrate. Shulz and co-workers (*8*) have shown that the k_{cat} rate for the elimination of 3-hydroxy-3-phenylpropanoyl-CoA is comparable to that of the physiological substrates. Consequently, the details of the mechanism and transition states are likely to be identical for the unsaturated physiological and phenyl-conjugated substrates of ECH.

A mobile loop of ECH of residues 113−119 moves out of the way to bind substrates and inhibitors larger than acetoacetyl-CoA. A comparison of this loop's position for the ECH·DAC-CoA and acetoacetyl-CoA complex shows the magnitude of the loop motion necessary for binding of the larger substrate (Figure 5). Previously, Engel et al. (*22*) determined the structure of the inhibitor octanoyl-CoA bound to ECH in an effort to understand what changes are necessary within the enzyme's active site to bind larger substrates. Octanoyl-CoA is a competitive inhibitor that lacks the *β*-hydroxy group necessary for it to be a substrate. Binding of the larger octanoyl-CoA caused the mobile loop to move from the position seen previously for bound acetoacetyl-CoA (*4*). However, the mobile loop became disordered. In our structure of ECH·DAC-CoA, we see electron density for the entire mobile loop (residues 113−119) in each of the six active sites within the crystallographic asymmetric unit (Figure 5). The physiological substrates of ECH have alkyl chains that range from four carbons (crotonyl-CoA) to 16 carbons (2-hexadecenoyl-CoA), with the V_{max}/K_m rate of reaction decreasing with an increase in the chain length (*33*). The requirement for the mobile loop to reorient itself for larger thiolester substrates is most likely an essential factor in controlling the relative reaction rate of substrates of varying chain length.

The structure that has been determined is the Michaelis complex for the addition reaction. An analysis of this structure allows a more thorough description of the chemical mechanism of the addition reaction. The model of the DAC-CoA substrate has low *B*-factors and very clean electron density maps, indicating a single conformation of the substrate in each of the six active sites. The crystallographic evidence of a single conformation of the substrate bound is noteworthy for the work reported in the following paper (*10*) that describes the polarization of ^{13}C NMR resonances of DAC-CoA bound to ECH. The substrate is polarized by interaction of the thiocarbonyl with the backbone amides of Gly^{141} and Ala^{98} as shown in Figure 4. A sequence alignment of all members of the ECH superfamily (*34*) reveals that Gly^{141} is nearly conserved, with a few notable exceptions that contain alanine at this position. The ECH site-directed mutant $Gly^{141} \rightarrow$ Pro, which lacks a hydrogen bond donor, has a 1 million-fold decrease in k_{cat} (*35*). However, Ala^{98} is not conserved to the same degree. An interesting observation from an alignment of the crotonase superfamily is that the flanking residues Gly^{97} and Asp^{99} are absolutely conserved. It appears that these residues are critical for placing the peptide plane between Gly^{97} and Ala^{98} in a specific orientation, thereby aligning the amide nitrogen of Ala^{98} in an optimal geometry for donation of its hydrogen bond to the thiocarbonyl. The strategy that ECH uses to polarize the thiolester substrate, and ultimately a transition state, is strikingly similar to those of the homologous proteins 4-chlorobenzoyl-CoA dehalogenase (*36*) and dienoyl-CoA isomerase (*37*) as well as other members of the crotonase superfamily (*34*). This structural homology was successfully manipulated by the protein engineering of 4-chlorobenzoyl-CoA into an enzyme with ECH activity (*38*). This further demonstrates a potential link in the evolution of function for members of the ECH enzyme superfamily (*39*).

On the basis of pH−rate profiles and the α-proton exchange rates of the wild type and site-directed mutants $Glu^{144} \rightarrow$ Gln and $Glu^{164} \rightarrow$ Gln, it has been argued that the active form of ECH at physiological pH exists when one carboxylate is neutral and one is negatively charged (*40*). A potential mechanism (adapted from ref *40*) is shown in Scheme 2, which starts with a protonated Glu^{164} in the E−S complex and ends with a protonated Glu^{144} in the E−P complex.

Although the E−S structure presented here was determined at pH 7.3, it cannot directly rule out this possibility. The observed hydrogen-bonding network could still exist with the amide hydrogens interacting with the lone pair electrons of a carboxylate oxygen in residues Glu^{144} and Glu^{164} that is protonated. However, if either of the glutamates is protonated, and therefore neutral, then it would have a hydrogen covalently bonded to one of its carboxylate oxygens. This hydrogen, if it exists, would not interact by H-bonding with any other residue in the enzyme's active site. From the structure of the E−S complex, the other question that arises involves the source of the proton for protonating C_2 of the substrate. The mechanism shown in Scheme 2 has the source of this proton as the carboxylate OE2 oxygen of Glu^{164} from the E−S complex. In the E−S structure with DAC-CoA bound, the average distance between this OE2 oxygen of Glu^{164} and the C_2 atom of DAC-CoA is 6.2 Å. The side chain of Glu^{164} would need to be shifted and reoriented dramatically to allow for the protonation of C_2 from this position.

From an inspection of the interactions of the oxygens of the Glu^{144} and Glu^{164} side chains, which are bridged by the catalytic water in the E−S structure, there is a distinct lack

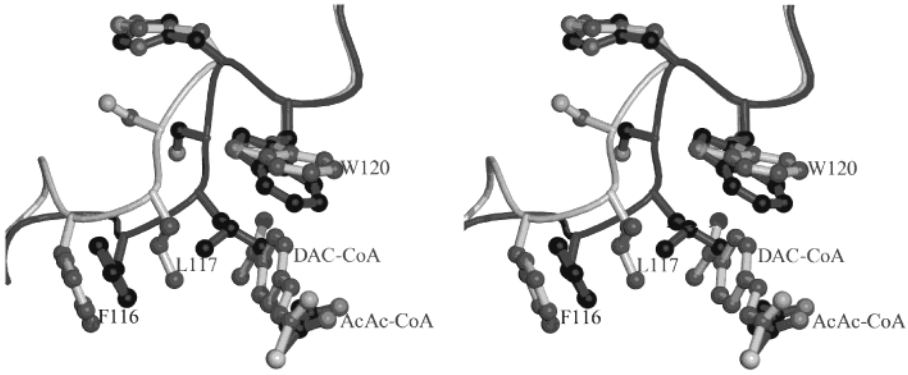

FIGURE 5: Hydrophobic binding pocket of the acyl portion of substrates shown in stereoview. Phe[116], Leu[117], and Trp[120] interact with bound DAC-CoA as part of a loop that has been shown to have alternate conformations. Comparison of the loop conformation of residues 113−120 with DAC-CoA bound (light gray) and acetoacetyl-CoA bound (*4*) (dark gray) to ECH. A least-squares fit was performed between all the α-carbon atoms of a monomer of ECH·DAC-CoA vs ECH·acetoacetyl-CoA. When DAC-CoA is bound to ECH, the loop of residues 113−120 is moved to increase the size of the hydrophobic binding pocket to accommodate the larger R group of DAC-CoA. This figure was created using the programs MOLSCRIPT (*23*), POVSCRIPT (E. Peisach and D. Peisach, unpublished program), and POVRAY (http://www.povray.org).

Scheme 2: ECH Mechanism with Glu[164] Initially Protonated

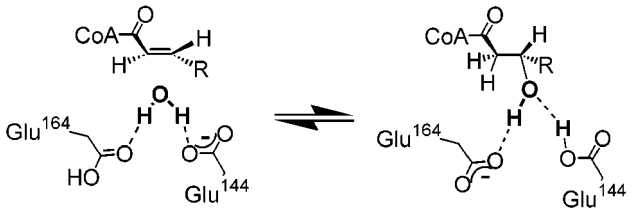

of any additional proton donor or hydrogen bond acceptor (Figure 3). This fact, together with the observation that the bound water is the closest source of a C_2 proton donor, leads to our hypothesis that the water is neutral and both carboxylates are ionized with formal negative charges. The absolute charge on each of these carboxylate groups is reduced from a value of −1 by direct H-bond interactions with backbone amides as shown in Figure 3. When one starts from this configuration of side chains, protons, and the catalytic water, the simplest model of catalysis is one in which all three atoms of the catalytic water end up in the product. The ECH·DAC-CoA structure is consistent with a *syn* addition of the catalytic water across the double bond (*1*), particularly in light of an absence of any other proton donor other than the catalytic water molecule. Although it has been suggested that β-elimination−addition reactions must be stepwise (*41*), we had interpreted kinetic isotope effect and isotope exchange data to be more consistent with a concerted ECH reaction (*2*, *3*). Once the structural perspective that our current ECH·DAC-CoA provides had been obtained, a possible mechanistic scenario has become evident that accommodates an E1cb stepwise mechanism and is still consistent with previous experimental results (*2*, *3*). A possible model will now be described by referring to the bottom path of Scheme 3, which shows a hypothetical E1cb carbanion mechanism. The ECH−substrate complex shown on the left of Scheme 3 is depicted directly from the ECH·DAC-CoA crystal structure. The atoms of the bridging water molecule are bold relative to the other atoms of the scheme for each species that is depicted. The first step of a carbanion stepwise addition is the formation of the C_3−oxygen bond in forming a carbanion intermediate.

During the formation of this intermediate, one of the original hydrogens of the catalytic water has been transferred to the carboxylate of Glu[164]. In the subsequent step, this same proton is transferred to C_2 of the product. Thus, this proton can give rise to primary deuterium isotope effects on both bond-forming steps of the E1cb mechanism. The primary deuterium isotope effect has been determined, and was previously attributed to the C_2 (de)protonation step (*2*, *3*). However, due to the current structural understanding, the mechanism proposed here suggests that this primary deuterium isotope effect could arise from the proton transfer between Glu[164] and the catalytic water molecule as well. During this step, the bound water molecule undergoes an O−H bond cleavage as the hydroxyl is added to form the carbanion intermediate. In this scenario, all observed isotope effects (*2*, *3*, *27*) would need to reflect the carbon−oxygen bond cleavage−formation step for the isotope effects to be self-consistent. It should be noted that the hypothetical situation described above of a carbanion intermediate breaks down if protons are supplied from another source, other than the three atoms of an incoming or departing water molecule.

An alternate description of the mechanism is one in which, following formation of the E−S complex, the three atoms of the catalytic water approach the double bond to form a four-membered cyclic transition state structure as depicted in the top path of Scheme 3. Although surprising, a precedent for a four-membered cyclic transition state structure has been reported (*42*) and reviewed (*43*) from the quantum-mechanics/molecular-mechanics (QM/MM) modeling of peptide hydrolysis by thermolysin. With ECH, a four-membered transition state mechanism may explain why this reaction is a *syn* addition, compared to the nonenzymatic β-addition−elimination reactions of thiolesters that have been shown to follow *anti* stereochemistry (*13*). In a hypothetical active site, it is feasible to have an enzyme that has *anti* stereochemistry with an arrangement of residues that have a pre-equilibrium deprotonation of the catalytic water, followed by a concerted addition reaction. However, if an essential element of the mechanism is a single four-membered transition state, then the *syn* stereochemistry will be enforced. An additional possibility to consider with a concerted mechanism is that upon binding the α,β-unsaturated substrate and a water

Scheme 3: ECH Mechanism with Both Carboxylates Deprotonated

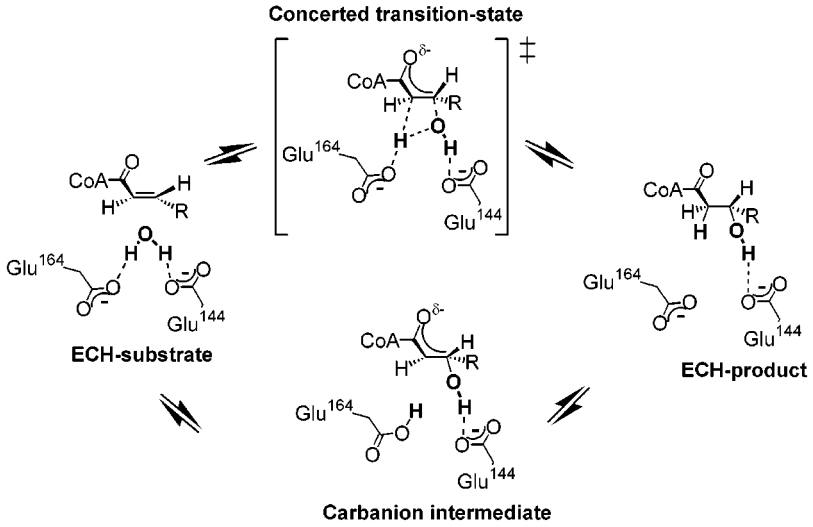

molecule, the water molecule may undergo a pre-equilibrium deprotonation. This species, with a protonated Glu[164] and Glu[144] hydrogen bonded to the OH^- group, would then react through a concerted addition mechanism. Although the pK_a values of the two carboxylates have not been directly measured, we can predict the relative values on the basis of the geometry of the carboxylate oxygen lone pair electron that is involved. Gandour and others (*24*, *25*, *44*) have argued that the *syn* orbital of a carboxylate should be 2−3 orders of magnitude more basic because it points into the plane of the V-shaped CO_2 compared to the *anti* orbital, which points away. Therefore, the pK_a of the Glu[164] carboxylate may be 2−3 units lower due to its *anti* electron pair involved in the hydrogen bond versus the *syn* hydrogen bond of Glu[144]. The deprotonation of water by the predicted weaker base Glu[164] is consistent with the mechanism after invoking microscopic reversibility. The back reaction, which is the elimination of water from the 3-hydroxy thiolester, would have the stronger acid Glu[164] available for removing the proton from C_2 of the substrate in the β-elimination reaction.

It should be noted that an additional scenario exists that allows one to reconcile the mechanisms shown in Scheme 3 with the prediction that the reaction proceeds with a single protonated carboxylate (*40*). For example, if Glu[164] is protonated in both the E−S and E−P complexes, and this proton is not directly involved in the reaction, then either path of Scheme 3 could be followed, where the three atoms of the catalytic water are added across the double bond. Theoretical approaches are being explored using the available information that define the ground state and transition state structures of the mechanism. Preliminary DFT/PM3 quantum calculations have yielded an intermediate consistent with the bottom path of Scheme 3 (*45*). Furthermore, attempts to add a single proton to the theoretical model of the E−S complex with both carboxylates initially deprotonated have led to the protonation of the incipient water molecule, not the unprotonated carboxylate oxygens (V. E. Anderson, unpublished observations).

The mechanism predicts specific interactions in the E−P complex. As in the E−S complex, the carboxylates of Glu[144] and Glu[164] are expected to be ionized in the E−P complex, without any need to invoke other residues directly in the catalysis of the addition−elimination reaction. The mechanistic scenario depicted in Scheme 2 predicts an alternate H-bonding pattern, where both Glu[144] and Glu[164] are directly interacting with the hydroxyl portion of the hydrated product in the E−P complex. The crystal structure determined with the competitive inhibitor acetoacetyl-CoA bound to ECH (*4*) is consistent with the former prediction, where the 3-oxo-C_3 oxygen of acetoacetyl-CoA was shown to be roughly where the 3-hydroxy group of the E−P complex is likely to be and is hydrogen-bonded to only Glu[144]. The 303 nm UV absorbance of bound acetoacetyl-CoA (*33*) indicates that it is bound as an enol. Also, the pH independence of the K_i for acetoacetyl-CoA (V. E. Anderson, unpublished observation) likewise indicates it is bound as the enol and is capable of H-bonding to the ionized form of Glu[144]. However, the enol resonance requires that the C_3 oxygen of acetoacetyl-CoA lay in the plane of the thioester carbonyl, while for the dehydration reaction, the C_3 oxygen of the product must be above the plane. As a result, the C_3−OH bond of the 3-hydroxy substrate would be orthogonal to the C_3−O double bond of acetoacetyl-CoA. It is predicted that this different position of the oxygen must influence the position of the H-bonded Glu[144].

The other species of the ECH mechanism that is of interest is the apo form of the enzyme. The original crystal structure of ECH was created with the competitive inhibitor acetoacetyl-CoA bound to five of the enzyme's six active sites of the physiological hexamer (*4*) as noted above. However, the sixth active site did not have inhibitor bound, and therefore serves as an apo structure of rat liver ECH. In this structure (PDB entry 1DUB), a water molecule bridges residues Glu[144] and Glu[164] just as in the ECH·DAC-CoA structure. This water likely becomes the catalytic water once the α,β-unsaturated substrate binds. Presumably, this same water must dissociate prior to, or be displaced by, the binding of the hydrated product for the reverse reaction to occur.

The crystal structure of ECH·DAC-CoA allows details of the mechanism to be deduced at atomic resolution. Furthermore, this structure is required to analyze experimental details and obtain estimates of substrate destabilization derived from ^{13}C NMR spectroscopy of ECH-bound substrates in the following paper (*10*). Ultimately, the combination of infor-

mation from kinetics (*2*, *3*, *7*, *8*), site-directed mutagenesis (*6*, *40*), spectroscopy (*5*, *32*), and atomic resolution structures of productive enzyme complexes will allow theoretical modeling of this enzyme-catalyzed reaction with unprecedented reliability. The mechanism of ECH, as is true of many enzymes (*46*), is likely to have an essential dynamic component to its catalytic efficiency. The E−S species is a ground state form of the enzyme. The other ground state forms, which can be attained by X-ray crystallography, are the E−P form and the apo form (see above). Spectroscopy of ECH-bound substrates also defines the ground state species of an enzyme mechanism (*5*, *32*). The next step in understanding the enzyme is to fill in the gaps of the mechanism by describing how the enzyme brings these ground state species to the transition state and potential carbanion intermediates of the reaction. One picture of enzyme dynamics, which would have a profound effect on the catalytic rate, is a compression of the catalytic water, which is poised between the two glutamates and C_3 of the thiolester substrate. In the E−S complex, the catalytic water is positioned within van der Waals contact with an oxygen−C_3 distance of 3.0 Å. The water's free lone pair of electrons is pointing directly at C_3 of the DAC-CoA substrate (Figure 3B). Furthermore, a synchronous shortening and geometric optimization of the hydrogen bonds between the thiolester carbonyl and the enzyme's backbone amides would polarize the substrate as the transition state was approached. Although this is merely a hypothetical picture, this level of understanding should be able to be attained by combining the crystallographic, kinetic, and spectroscopic experimental results with novel theoretical approaches that include a treatment of enzyme dynamics in catalysis.

ACKNOWLEDGMENT

We thank Professor R. Wierenga for supplying us with the coordinates of ECH with acetoacetyl-CoA bound prior to publication. B.J.B. thanks Professor D. Ringe for laboratory resources and for helpful discussions.

REFERENCES

1. Willadsen, P., and Eggerer, H. (1975) *Eur. J. Biochem. 54*, 247−252.
2. Bahnson, B. J., and Anderson, V. E. (1989) *Biochemistry 28*, 4173−4181.
3. Bahnson, B. J., and Anderson, V. E. (1991) *Biochemistry 30*, 5894−5906.
4. Engel, C. K., Mathieu, M., Zeelen, J. P., Hiltunen, J. K., and Wierenga, R. K. (1996) *EMBO J. 15*, 5135−5145.
5. Wu, W. J., Anderson, V. E., Raleigh, D. P., and Tonge, P. J. (1997) *Biochemistry 36*, 2211−2220.
6. Kiema, T. R., Engel, C. K., Schmitz, W., Filppula, S. A., Wierenga, R. K., and Hiltunen, J. K. (1999) *Biochemistry 38*, 2991−2999.
7. D'Ordine, R. L., Bahnson, B. J., Tonge, P. J., and Anderson, V. E. (1994) *Biochemistry 33*, 14733−14742.
8. Mao, L.-F., Chu, C., and Schulz, H. (1994) *Biochemistry 33*, 3320−3326.
9. D'Ordine, R. L. (1995) in *Chemistry*, pp 145, Brown University, Providence, RI.
10. D'Ordine, R. L., Pawlak, J., Bahnson, B. J., and Anderson, V. E. (2002) *Biochemistry 41*, 2630−2640.
11. Person, N. B. (1981) Ph.D. Thesis, State University of New York at Buffalo, Buffalo, NY.
12. Hanson, K. D., and Rose, I. A. (1975) *Acc. Chem. Res. 8*, 1.
13. Mohrig, J. R., Moerke, K. A., Cloutier, D. L., Lane, B. D., Person, E. C., and Onasch, T. B. (1995) *Science 269*, 527−529.
14. Hass, G. M., and Hill, R. L. (1969) *J. Biol. Chem. 244*, 6080−6086.
15. Jancarik, J., and Kim, S. H. (1991) *J. Appl. Crystallogr. 24*, 409−411.
16. Otwinowski, Z., and Minor, W. (1997) *Methods Enzymol. 276*, 307−326.
17. Collaborative Computational Project No. 4 (1994) *Acta Crystallogr. D50*, 760−763.
18. Brunger, A. T. (1992) *X-PLOR Version 3.1. A system for X-ray Crystallography and NMR*, Yale University Press, New Haven, CT.
19. Brunger, A. T. (1992) *Nature 355*, 472−474.
20. Jones, T. A., Zou, J. Y., Cowan, S. W., and Kjeldgaard, M. (1991) *Acta Crystallogr. A47*, 110−119.
21. Brunger, A. T., Adams, P. D., Clore, G. M., Delano, W. L., Gros, P., Grosse-Kunstleve, R. W., Jiang, J.-S., Kuszewski, J., Nilges, N., Pannu, N. S., Read, R. J., Rice, L. M., Simonson, T., and Warren, G. L. (1998) *Acta Crystallogr. D54*, 905−921.
22. Engel, C. K., Kiema, T. R., Hiltunen, J. K., and Wierenga, R. K. (1998) *J. Mol. Biol. 275*, 847−859.
23. Kraulis, P. J. (1991) *J. Appl. Crystallogr. 24*, 946−950.
24. Rebek, J. J. (1990) *Angew. Chem., Int. Ed. Engl. 29*, 245−255.
25. Gandour, R. D. (1981) *Bioorg. Chem. 10*, 169−176.
26. Hol, W. G. (1985) *Adv. Biophys. 19*, 133−165.
27. Bahnson, B. J. (1991) Ph.D Thesis, Brown University, Providence, RI.
28. Walsh, M. A., Schneider, T. R., Sieker, L. C., Dauter, Z., Lamzin, V. S., and Wilson, K. S. (1998) *Acta Crystallogr. D54*, 522−546.
29. Steiner, R. A., Rozeboom, H. J., de Vries, A., Kalk, K. H., Murshudov, G. N., Wilson, K. S., and Dijkstra, B. W. (2001) *Acta Crystallogr. D57*, 516−526.
30. Bonvin, A. M., and Brunger, A. T. (1995) *J. Mol. Biol. 250*, 80−93.
31. Zhang, E., Brewer, J. M., Minor, W., Carreira, L. A., and Lebioda, L. (1997) *Biochemistry 36*, 12526−12534.
32. D'Ordine, R. L., Tonge, P. J., Carey, P. R., and Anderson, V. E. (1994) *Biochemistry 33*, 12635−12643.
33. Waterson, R. M., and Hill, R. L. (1972) *J. Biol. Chem. 247*, 5258−5265.
34. Holden, H. M., Benning, M. M., Haller, T., and Gerlt, J. A. (2001) *Acc. Chem. Res. 34*, 145−157.
35. Bell, A. F., Wu, J., Feng, Y., and Tonge, P. J. (2001) *Biochemistry 40*, 1725−1733.
36. Benning, M. M., Taylor, K. L., Liu, R. Q., Yang, G., Xiang, H., Wesenberg, G., Dunaway-Mariano, D., and Holden, H. M. (1996) *Biochemistry 35*, 8103−8109.
37. Modis, Y., Filppula, S. A., Novikov, D. K., Norledge, B., Hiltunen, J. K., and Wierenga, R. K. (1998) *Structure 6*, 957−970.
38. Xiang, H., Luo, L., Taylor, K. L., and Dunaway-Mariano, D. (1999) *Biochemistry 38*, 7638−7652.
39. Gerlt, J. A., and Babbitt, P. C. (2001) *Annu. Rev. Biochem. 70*, 209−246.
40. Hofstein, H. A., Feng, Y., Anderson, V. E., and Tonge, P. J. (1999) *Biochemistry 38*, 9508−9516.
41. Gerlt, J. A., and Gassman, P. G. (1992) *J. Am. Chem. Soc. 114*, 5928−5934.
42. Antonczak, S., Monard, G., Ruiz-Lopez, M. F., and Rivail, J. (1998) *J. Am. Chem. Soc. 120*, 8825−8833.
43. Monard, G., and Merz, K. M., Jr. (1999) *Acc. Chem. Res. 32*, 904−911.
44. Gu, Z., Drueckhammer, D. G., Kurz, L., Liu, K., Martin, D. P., and McDermott, A. (1999) *Biochemistry 38*, 8022−8031.
45. Pawlak, J., Bahnson, B. J., and Anderson, V. E. (2002) *Nukleonika* (in press).
46. Wilson, E. K. (2000) *Chem. Eng. News 78* (29), 42−45.

BI015844P